Assessing the Performance, Reliability, Economic, and Environmental Impact of Photovoltaic Systems Installation Parameters in Harsh Climates: Case Study Iraq

Peer-reviewed author version

Hameed, Mohammed Adnan; KAAYA, Ismail; Alias, Qais Matti; KYRANAKI, Nikoleta; DAENEN, Michael; DE JONG, Richard; MORLIER, Arnaud; Scheer, Roland & Gottschalg, Ralph (2024) Assessing the Performance, Reliability, Economic, and Environmental Impact of Photovoltaic Systems Installation Parameters in Harsh Climates: Case Study Iraq. In: Solar RRL, 8 (18) (Art N° 2400455).

DOI: 10.1002/solr.202400455
Handle: http://hdl.handle.net/1942/43678

Assessing the Performance, Reliability, Economic, and Environmental Impact of PV Systems Installation Parameters in Harsh Climates: Case Study Iraq

Mohammed Adnan Hameed[a,b,c], Ismail Kaaya[d,e,f], Nikoleta Kyranaki[d,e,f], Richard de Jong[d,e,f], Michaël Daenen[d,e,f], Arnaud Morlier [d,e,f], Qais Matti Alias[g], Roland Scheer[b] and Ralph Gottschalg[c]

[a] Ministry of Oil -SCOP, Baghdad, Iraq

[b] Martin-Luther-University Halle-Wittenberg, Halle, Germany

[c] Fraunhofer Center for Silicon Photovoltaics CSP, Halle, Germany

[d] Imec, imo-imomec, Thor Park 8320, 3600 Genk, Belgium,

[e] Hasselt University, imo-imomec, Martelarenlaan 42, Hasselt, Belgium Belgium,

[f] EnergyVille, imo-imomec, Thor Park 8320, 3600 Genk, Belgium,

[g] Retired Faculty Member in the University of Technology, Baghdad, Iraq

Abstract

This study examines the impact of various photovoltaic (PV) installation parameters including tilt angle, azimuth angle, row pitch, height above ground, and albedo effect on the operating conditions of PV modules installed in harsh site conditions, focusing on irradiance levels and module temperature. It evaluates how these parameters influence the degradation rate and, subsequently, the overall lifetime of PV modules. The variation in PV module lifetime is then correlated with lifetime energy generation, economic factors, and environmental impact. A novel optimization strategy for PV systems is proposed, which considers three indicators: lifetime energy yield, levelized cost of electricity (LCOE), and greenhouse gas (GHG) emission factors, rather than solely economic aspects as is common practice. The study's findings demonstrate that installation parameters significantly affect climate stressors and module lifetime, necessitating their consideration in PV system optimization. For instance, in the simulated location, higher tilt angles are recommended to reduce stress levels on PV modules, thereby extending their lifespan. This strategic choice also mitigates losses due to soiling, balancing optimal energy yield with prolonged system lifetime and environmental considerations. The study highlights that height and albedo are the most sensitive installation parameters, especially for bifacial modules. Variations in these parameters could result in lifetime differences of over 4 and 8 years, respectively, leading to energy yield differences of 20.8% and 46.7%. Using the proposed optimization strategy, an optimal albedo of 0.5 was identified, aligning with the albedo of desert sand, indicating that albedo boosters may not be necessary in desert climates. Overall, this research provides valuable insights for PV designers and stakeholders, stressing the importance of considering long-term and environmental impacts alongside economic factors when optimizing PV system designs

Keywords:

Degradation rate, installation parameters, performance, LCOE, Greenhouse gas emissions, PV systems, harsh climate, Iraq.

1. Introduction

The energy output of PV installations depends on several factors such as the tilt and azimuth angles, the height or elevation of the PV modules from the ground, and the spacing between the PV strings. Additionally, the type of tracking – single or dual axis, the ground reflectance (albedo) and the type of PV technology also impact the energy output of the PV systems. PV systems designers focus on a design that produces the maximum energy output (usually determined by annual yield output) to optimize profits. Furthermore, various studies have been conducted to assess the optimal parameters for PV installations based on energy output [1], [2], [3], [4], [5], [6], [7], [8]. However, a crucial aspect often overlooked is that conditions conducive to maximum annual output may subject PV modules to higher stresses especially higher operating temperatures and UV exposure. This could impact the PV module reliability negatively by accelerating the degradation mechanisms such as encapsulation discolouration, Light and elevated temperature-induced degradation (LeTID) [9], Ultraviolet induced degradation (UV-LID) [10], [11]— increasing the degradation rate, and lowering the PV module's lifetime.

While numerous studies have demonstrated the impact of tilt angle on soiling rates [12], [13], [14], [15], [16], few have examined the influence of installation parameters on the long-term degradation rate of PV modules. To the best of our knowledge, only authors in [17], [18] and [19] have correlated some installation parameters on operating conditions and long-term degradation of PV modules. For instance, simulations in [17] revealed the impact of tilt angle on degradation rates, while [18] Highlighted higher operating temperatures in tracking PV systems than fixed systems, further showing that tracked systems degrade more rapidly. Additionally, experimental findings in [19] from outdoor installed PV modules in the Middle East and North Africa (MENA) hot desert region demonstrated that modules tilted at 25° exhibited higher defects compared to tilt angles 15° and 90° indicating a dependence of installation parameters on module degradation. However, although the mentioned studies reveal the impact of the tilt angle on degradation rates, thorough investigation and identification of the various degradation mechanisms are missing.

The insights from these studies motivated our comprehensive assessment of various installation parameters on the performance and reliability of PV systems. In contrast to prior works, our study evaluates different parameters such as tilt angle, row pitch, height from the ground, and the influence of ground surface albedo. Furthermore, we incorporate simulations of PV systems with multiple strings to consider mismatch and inter-row shading effects.

Moreover, our analysis incorporates three crucial variables: (**a**) lifetime energy yield, (**b**) levelized cost of electricity, and (**c**) greenhouse gas emissions factor, to define the optimal installation design. Notably, prior studies have typically neglected the effect of CO_2 emissions on PV design optimization. By integrating these three factors, we aim to enhance the bankability of solar projects, aiming to increase lifetime energy production, reduce costs, and minimize greenhouse gas emissions for the PV system to be deployed in harsh site conditions like those in Iraq.

Our focus is on desert climate zones primarily due to their high solar irradiation levels, which are advantageous for solar power generation [20], [21]. However, these regions also present challenging conditions such as high environmental temperatures, significant temperature fluctuations between day and night, and dusty surroundings, among other factors. These harsh operating conditions have a negative impact on the performance and reliability of PV modules [22], [23], [24], [25], [26], [27], [28]. To ensure that PV modules can withstand these conditions and maintain a lifetime of at least thirty years, various parameters need to be considered, spanning from the bill of materials to installation design considerations. The authors in [29] have introduced PV module designs tailored for desert applications, often referred to as the "desert label". Our contribution aims to enhance PV reliability in desert climates by focusing on PV design parameters.

2. Methodology

2.1 Energy yield modelling

We deployed IMEC's PV energy yield simulations framework shown in Figure 1. The framework is bottom-up physics-based and includes Ray tracing/illumination, optical, thermal, and electrical models. The ray tracing /illumination model uses weather data to calculate the plane-of-array irradiation (Gpoa) on all PV elements. The ray tracing model allows the simulation of the effects of PV configurations (e.g. module tilt, azimuth, row spacing/pitch). The optical and thermal model allows for simulation of the material properties (e.g. module layers properties, reflective mounting structure, ground covers-albedo). The detailed description of the modelling framework has been described elsewhere in [21], [30], [31], [32]. Using this physics-based modelling framework, we can analyze the impact of PV installation parameters on Gpoa, module temperature, and energy yield.

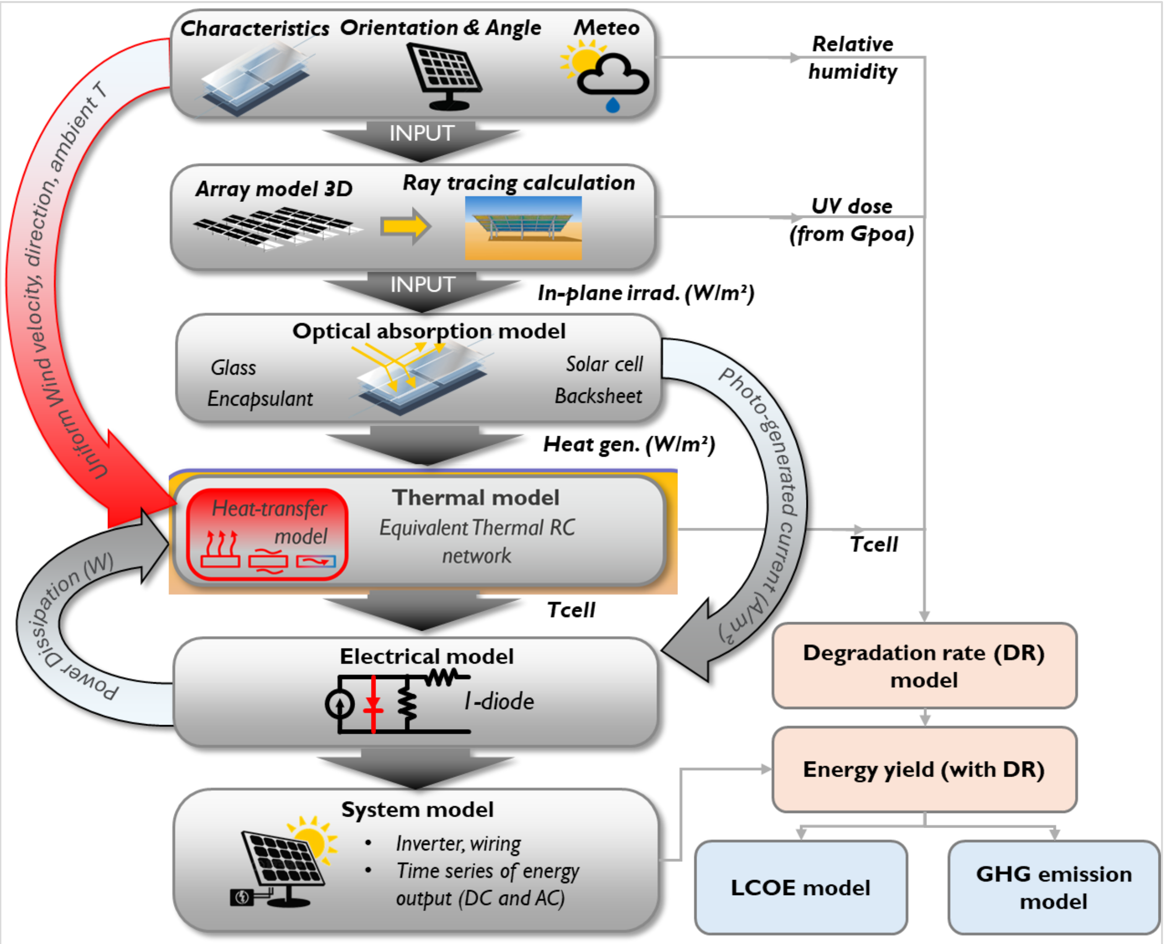

Figure 1. Schematic overview of IMEC's PV energy yield simulations framework with degradation rate, LCOE and GHG emission models integration

From the framework, the total annual yield without degradation impact is calculated. It should be noted that in this study, DC yield is utilized for all financial and environmental calculations. To calculate the lifetime energy yield considering the degradation rates for a given scenario the following expression is used:

$$EY_{LT} = \sum_{\mathrm{n}=1}^{\mathrm{n}} EY_{YI}(1-\mathrm{DR})^{\mathrm{n}} \qquad \text{Eq. (1)}$$

Where; EY_{LT} is the lifetime energy yield, EY_{YI} is the first-year energy yield, DR is the annual degradation rate and n is the lifetime (years) of the PV system.

2.2 Degradation rate modelling

To evaluate the non-reversible degradation rate, we applied the model proposed in [33]. The total degradation rate of power (DR_T[%/year]) is estimated as a function of specific degradation mechanisms/processes based on the applied climatic stresses as [33]:

$$DR_T = A_N \cdot (1+\mathrm{DR_H})(1+\mathrm{DR_P})(1+DR_{Tm}) - 1 \qquad \text{Eq. (2)}$$

Where DR_H, DR_P and DR_{Tm} are the degradation rates for hydrolysis, photodegradation, and thermomechanical degradation, respectively. These rates are evaluated as functions of environmental stressors as [33], [34]:

$$\mathrm{DR_H(T, RH)} = \mathrm{A_H} \cdot \exp\left(\frac{-\mathrm{E_{aH}}}{\mathrm{k_B} \cdot \mathrm{T}}\right) \cdot \mathrm{RH^n} \qquad \text{Eq. (3)}$$

$$\mathrm{DR_P(UV, T, RH)} = \mathrm{A_p} \cdot \mathrm{UV^y} \cdot (1 + \mathrm{RH^{n_1}}) \cdot \exp\left(\frac{-\mathrm{E_{aP}}}{\mathrm{k_B} \cdot \mathrm{T}}\right) \qquad \text{Eq. (4)}$$

$$\mathrm{DR_{Tm}(\Delta T, T_{max})} = \mathrm{A_T} \cdot (\Delta \mathrm{T} + 273)^{\mathrm{x}} \cdot \mathrm{C_r} \cdot \exp\left(\frac{-\mathrm{E_{aT}}}{\mathrm{k_B} \cdot \mathrm{T_{max}}}\right) \qquad \text{Eq. (5)}$$

Here , k_B (8.62×10^{-5} eV/K) is the Boltzmann constant, T [Kelvin] annual average module temperature, T_{max} [Kelvin] is the annual average maximum temperature of the module, ΔT is the annual average cyclic temperature of the module, UV [kWh/m^2] is the total annual UV dose, RH[%] annual average relative humidity, C_r[cycles/year] annual temperature cycling frequency (assumed as 1 cycle per year). Definitions of other model parameters and values used are presented in Table 1 below.

Table 1: Definition of model parameters and values used in degradation rate simulation.

Parameter	Quantity
A_N normalization constant of the physical quantities	1 $year^{-2}$
A_H exponential coefficient for hydrolysis	$4.91e7\ year^{-1}$
A_P exponential coefficient for photodegradation	$7.3e7\ (kWh/m^2)^{-1}$
A_T - exponential coefficient for thermomechanical degradation	$2.04\ cycle^{-1}$
E_{aH}, E_{aP} and E_{aT} [eV] activation energies, for hydrolysis, photodegradation and thermomechanical degradation respectively	Simulated as a distribution
n, n_1, y and x are model parameters that describe the effect of RH	$n = 1.9, n_1 = 0.1,\ y = 0.63$ and $x = 2.04$

The parameter in the models most closely associated with the PV bill of materials, and arguably the most critical one is the activation energy [35]. While other model parameters are adopted as presented in [33], [35], since we're simulating a different PV module compared to those in [33], [35], the activation energies

(E_{aH}, E_{aP} and E_{aT}) must be adjusted. Given the absence of historical degradation data for the specific module under evaluation, we employed a statistical approach. This involved utilizing a population of over 1000 different activation energies to conduct a Monte Carlo simulation. Through the utilization of a non-central F distribution continuous random variable generator [36] and imposition of boundary conditions for activation energies related to each degradation mechanism [33], [35], [37], [38], a distribution for E_{aH}, E_{aP} and E_{aT} was generated.

2.3 Greenhouse gas (GHG) emission factor modelling

A simplified model, based on the work of Louwen et al.[39], evaluates the greenhouse gas (GHG) emission factor (gCO2-eq/kW h). This factor is related to producing a PV system and is expressed per unit of PV system capacity (gCO2-eq/kWp). It is calculated by summing all the CO2-eq emissions originating during production, transport, installation, operation, and end-of-life treatment as;

$$\mathrm{G_{elec}} = \frac{G_{prod} + G_{tran} + G_{ins} + G_{EOL}}{\sum_{\mathrm{n}=1}^{\mathrm{n}} E_{yield}(1 - \mathrm{DR})^{\mathrm{n}}} \qquad \text{Eq.(6)}$$

Where; $\mathrm{G_{elec}}$ is the GHG emission factor, G_{prod} is the GHG emission during production in gCO2-eq/kWp, G_{tran} is GHG emission during transportation in gCO2-eq/kWp, G_{ins} GHG emission during installation in gCO2-eq/kWp and G_{EOL} is the GHG emission during the end of life in gCO2-eq/kWp. E_{yield} is the annual energy yield, DR is the annual degradation rate (%/year) and n is the lifetime (years) of the PV system.

The values of the different emission components used in the study are shown in Table 2.
$\mathrm{G_{prod}}$ are assumed based on the values provided in [39], [40], [41], [42] for modules produced in China.
$\mathrm{G_{tran}}$ and $\mathrm{G_{ins}}$ are assumed based on the transportation and installation conditions in Iraq. Additionally, the balance of system emissions is included in the $\mathrm{G_{ins}}$ component. Since no information is available about $\mathrm{G_{EOL}}$ it is neglected in this study.

Table 2. Values used in GHG emission factor calculations based on [39], [40], [41], [42].

Item	Cost
G_{prod}	750 $kgCO_2$-eq/kWp
G_{tran}	45 $kgCO_2$-eq/kWp
G_{ins}	125 $kgCO_2$-eq/kWp
G_{EOL}	-
E_{yield}, DR and n	Evaluated based on the installation parameters

2.4 Levelized cost of electricity (LCOE) modelling

The LCOE is estimated as [43]:

$$\mathrm{LCOE} = \frac{\text{Total Lifecycle Cost}}{\text{Total Lifetime Energy Production}} \qquad \text{Eq.(7)}$$

$$\mathrm{LCOE} = \frac{\mathrm{CAPEX} + \sum_{\mathrm{n=1}}^{\mathrm{n}} \frac{\mathrm{OPEX}}{(1+\mathrm{r})^{\mathrm{n}}}}{\sum_{\mathrm{n=1}}^{\mathrm{n}} \frac{Eyield \times (1-\mathrm{DR})^{\mathrm{n}}}{(1+\mathrm{r})^{\mathrm{n}}}} \qquad \text{Eq.(8)}$$

Where CAPEX is the capital expenditure (USD/kWp), OPEX is the operation expenditure (USD/kWp), DR is the degradation rate (%/year), Eyield is the annual energy yield (kWh), r is the discount rate (%) and n is the lifetime (years) of the PV system.

In this study, the CAPEX is subdivided into (a) initial investments/cost which includes transportation costs, administrative costs, labour costs, (b) PV module costs, (c) land costs – assuming the acquisition of land at the outset of the project and (d), mounting structure cost. The costs of the mounting structure are divided into fixed costs and costs adjusted according to height, in order to simulate the dependence of PV system costs on height. Therefore, the CAPEX is the two costs of all these sub-divisions. The OPEX is subdivided into (a) general PV system operation costs which include the cleaning costs, labour costs and (b) inverter replacement costs. The inverter replacement costs were separated since the lifetime of the inverters is shorter than those of the PV modules and depending on the module lifetime, the inverter's replacement costs will be different [44]. Table 3 defines the cost parameters used in this work.

Table 3. Cost breakdown used in LCOE calculations.

Item	Cost
Initial investments	10.13 USD/kWp
PV module	0.25 USD/Wp
Land costs	5 USD/m^2
Mounting structures fixed (str_fixed) Height-adjusted mounting structures	70.0 USD/kWp str_fixed + (1/3)*str_fixed*sys_height
General PV system operation (initial OPEX)	28.82 USD /kWp
Inverter replacement	51.05 /kWp
Discount rate (r)	2 %

2.5 Simulated scenarios

2.5.1 Details of the PV system simulated.

In this study, we simulated an 8.3kWp PV system comprising 5 strings, each consisting of 25 modules. Each module includes 132 half-cut bifacial cells (refer to Figure 2). The datasheet parameters of the simulated module are detailed in Table 4. The simulated system is assumed to be installed at a latitude of 33.011° and longitude of 44.385° in Baghdad. Typical Meteorological Year (TMY) data obtained from PVGIS [45] was utilized in the simulation (more specifically we used the PVGIS-SARAH2 2005 -2020 database).

Table 4. Datasheet parameters of the simulated PV module

Parameter	**Value**
Peak Power Watts-P_{MAX} (Wp)*	665
Maximum Power Voltage-V_{MPP} (V)	38.30
Maximum Power Current-I_{MPP} (A)	17.39
Open Circuit Voltage-V_{OC} (V)	46.10
Short Circuit Current-I_{SC} (A)	18.50
Temperature Coefficient of P_{MAX}	- 0.34%/°C
Temperature Coefficient of V_{OC}	- 0.25%/°C
Temperature Coefficient of I_{SC}	0.04%/°C
Module dimensions	2384×1303×35 mm

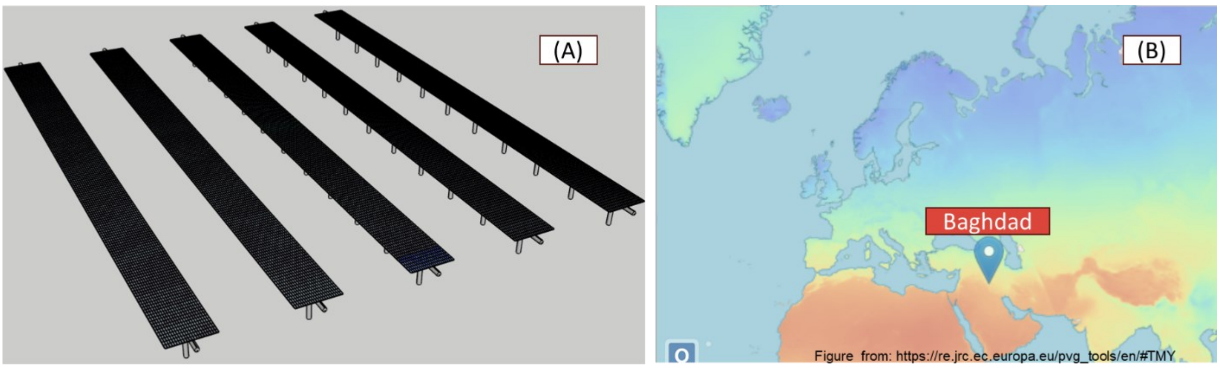

Figure 2. SketchUp model (A)of the simulated PV system and Map (B) highlighting the location of the simulated PV system. The map is a snapshot from PVGIS [45].

2.5.2 Details of the simulated installation parameters

We evaluated five primary installation parameters illustrated in Figure 3: (a) azimuth, (b) tilt angle, (c) row pitch, and (d) elevation/height from the ground, across five distinct scenarios (S):

- S1: Varied PV azimuth and different tilt angles.

- S2: Varied tilt angles at optimal azimuth.
- S3: Varied row pitch at optimal tilt angle and azimuth.
- S4: Varied PV system elevated height at optimal tilt angle and azimuth.
- S5 - Varied albedo at optimal tilt angle and azimuth.

In the analysis, each scenario is considered independently, meaning the selection of fixed parameters varies from one scenario to another. Our goal is to examine deviations for each scenario based on the standard optimization strategy of first-year yield while also considering the most realistic installation parameters.

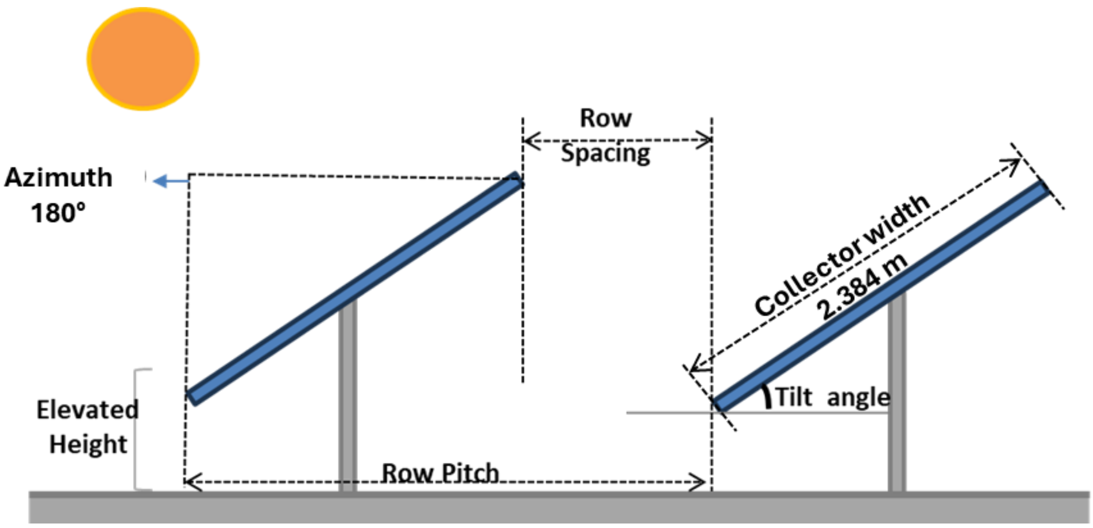

Figure 3 Schematic showing the different installation parameters. Note that in all simulation scenarios, the collector width remained constant.

Azimuth denotes the horizontal direction in which solar panels are oriented. Ideally, for optimal energy production, solar panels should directly face the sun at its zenith for a specific location. Also, it's expressed as an angle in degrees relative to true north, measured clockwise from north (0° azimuth), through east (90° azimuth), south (180° azimuth), and west (270° azimuth). Tilt angle refers to the angle at which solar panels are positioned relative to the horizontal plane. This angle affects the amount of sunlight the panels receive and varies based on factors such as latitude and seasonal sun path. Row pitch refers to the spacing between rows of solar panels in a ground-mounted installation. It determines the balance between maximizing land usage and minimizing shading between rows. Elevation or height from the ground refers to the distance between the bottom edge of the solar panels and the ground surface. This parameter is important for accessibility, maintenance, and ensuring proper clearance for vegetation or obstacles underneath the array. For bifacial PV modules, the height from the ground impacts the rear irradiation and hence the bifacial gain of the PV modules. That is the bifacial gain increases with increasing height from the ground [44], [45].

2.5.3 Benchmarking the economic impact of installation parameters

To avoid a biased evaluation of LCOE, we initially presume an ideal design aimed at maximizing the first-year energy yield, without accounting for degradation. This design is tailored to meet a household's energy consumption requirements as illustrated in Figure 4. Any alterations made to installation parameters deviate from this optimal setup. Subsequently, we evaluate the supplementary modules and land surface necessary to generate an equivalent energy output to the optimal design, thereby fulfilling the household's energy demands. Consequently, these adjustments influence the CAPEX and consequently impact the LCOE. In the study, we have considered a regular triangular flat terrain land plot oriented in the direction of the five strings/arrays without complex features, which facilitated the fitting of modules without the need for specialized software.

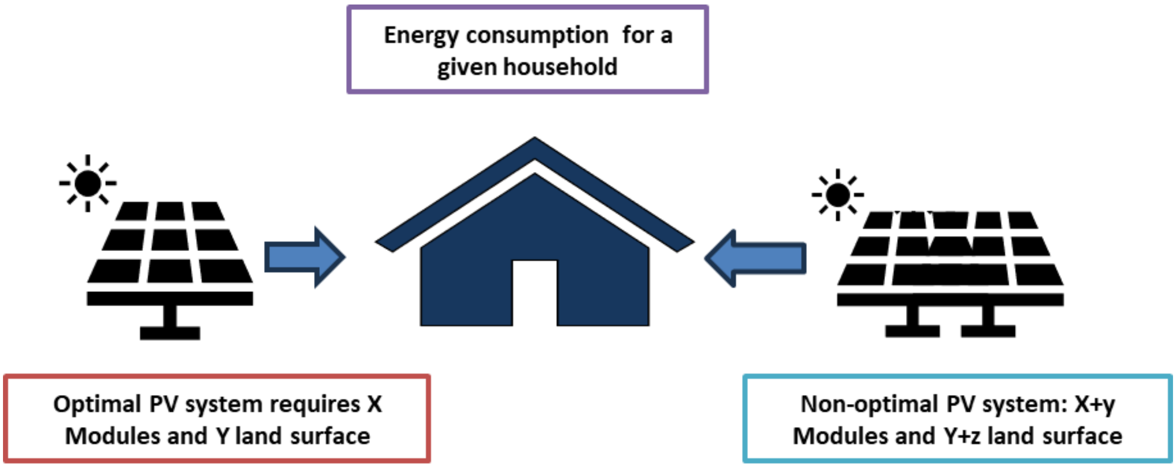

Figure 4. A diagram illustrating the optimization process of matching energy demand with PV modules and land. The "Optimal PV system" denotes the system parameters that fulfil annual energy needs based on annual yield without factoring in.

2.5.4 Statistical metrics to benchmark the impact of installation parameters

To assess the differences in energy yield, degradation rate, LCOE, and GHG emission factor resulting from various installation parameters, two metrics are employed: absolute change and percentage change, calculated as follows:

$$\text{Absolute change} = \mathrm{V_x} - \mathrm{V_{ref}} \qquad \text{Eq.(9)}$$

$$\text{Percentage change} = 100 \cdot \frac{\mathrm{V_x} - \mathrm{V_{ref}}}{\mathrm{V_{ref}}} \qquad \text{Eq.(10)}$$

Here $\mathrm{V_x}$ represents the performance indicator (such as energy yield, degradation rate, LCOE, etc.) of the installation parameter being evaluated, while $\mathrm{V_{ref}}$ stands for the reference installation parameter.

2.6 Soiling ratio simulation

The H.S.U (Humboldt State University, CA USA) model [46] is used to assess the effect of soiling according to the tilt angle and how this affects the energy yield. The models are implemented in an open-source PV simulation tool known as PVlib [47]. The model includes the effect of tilt angle (θ) and particulate matter (PM) data as:

$$m(d) = (v_{10-2.5} \cdot PM_{10-2.5}(d) + v_{2.5} \cdot PM_{2.5}(d)) \cdot t \cdot \cos(\theta) \qquad \text{Eq.(11)}$$

Where the m(d) is mass accumulation for a given day d, $v_{10-2.5}$ and $v_{2.5}$ are the static deposition velocities **t** is the factor used to convert the variables from a one-second interval into a daily value. The subscript 10–2.5 indicates that only particles with diameters within 10μm and 2.5μm are considered. $PM_{10-2.5}$ is therefore the difference between the PM_{10} and $PM_{2.5}$ concentrations. The daily mass accumulation (m) is then converted into a cumulative mass accumulation (w), which is reset to 0 on days in which the precipitation intensity is higher than a given threshold. The model parameters used in this work are $v_{10-2.5}$ (0.039) and $v_{2.5}$ (0.008) according to [48] and the cleaning threshold of 5 mm /day according to [49].

The daily soiling loss (SL), expressed in %, is calculated as:

$$SL(d) = 34.37 \cdot \mathrm{erf}\big(0.17 \cdot w(d)\big)^{0.8473} \qquad \text{Eq.(12)}$$

For the soiling evaluation, rainfall data was sourced from the Copernicus Climate Change Service [50] in daily averages. The PM data were obtained at 3-hour intervals from the EAC4 (ECMWF Atmospheric Composition Reanalysis 4) of the Copernicus Atmosphere Monitoring Service (CAMS) Atmosphere Data Store (ADS) [51]. Historical data spanning five years from 2015 to 2020 was employed to evaluate historical trends.

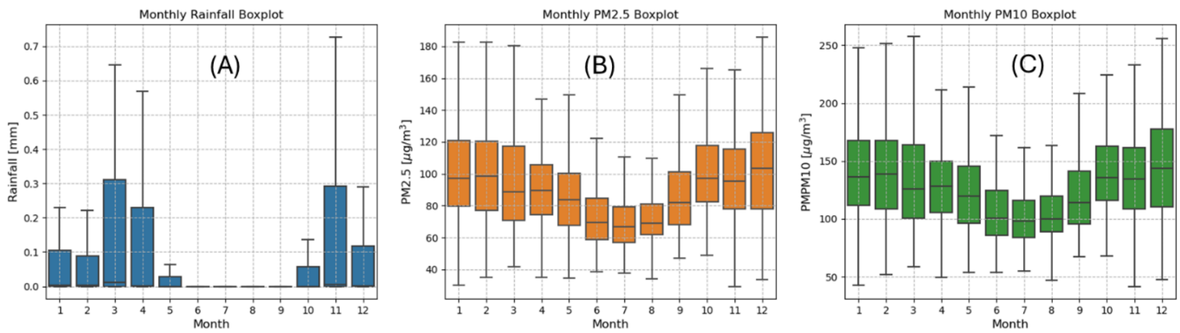

Figure 5. Monthly boxplots showing rainfall/precipitation (A), PM2.5 (B) and PM10 (C). All data represent 5 years time-series of the years 2015 to 2020 for Baghdad. (During the boxplot, outliers were removed).

2.7 Albedo measurement and impact on module temperature

The experimental setup was designed to explore the influence of varying ground albedo on the temperature of photovoltaic (PV) modules and its subsequent impact on module lifetime, employing degradation models. Three types of ground cover were chosen: grass, sand, and white polymer. Albedo and module temperature were measured for each ground cover.

Albedo measurements were conducted using albedometers equipped with two horizontal irradiance sensors: one facing the sky and the other facing the ground, depicted in Figure 6(A) and (B). Albedo was determined as the ratio of ground-facing pyranometer irradiance to sky-facing pyranometer irradiance. In this study, we refer to the measured albedo as the effective albedo. This term is used because, during the experiment, the pyranometer's field of view might be including some portions of exposed sand, given the grass and polymer fabrics did not cover a sufficiently large area, as illustrated in Figure 6.

The existing PV array was utilized, and different ground covers were applied to an area of approximately 4X4 modules in both the x and y directions. Temperature measurements were taken solely for the middle module of each ground cover location. Temperature sensors (thermocouples) were affixed to the back surface of the PV module(s), as illustrated in Figure 6(E), with two thermocouples per module to accommodate ground reflection inconsistencies. The PV modules were arranged at a fixed tilt angle to ensure uniform irradiance, with a string selected to mitigate shading effects. Each ground cover was positioned beneath a group of selected modules to maintain uniform incident solar radiation throughout the experiment. Continuous temperature data collection from the PV modules was carried out over approximately one week.

Figure 6. Effective albedo measurement for a white polymer (A) and for grass fabric (B). Module temperature measurement for grass fabric (C), and for white polymer (D). Thermocouple placement (E). The data was collected for the tracked tilt PV system.

3. Results and discussion

3.1 S1: Varied PV azimuth and different tilt angles

In this scenario, we conducted simulations to assess the energy yield under various azimuths (named orientations in this study) and tilt angles, aiming to identify the most effective combination. Throughout these simulations, the albedo, row pitch, and elevation of the modules remained constant at 0.20, 15.0 meters, and 2.0 meters, respectively. Figure 7 illustrates the simulated annual energy yield across different orientations and tilt angles. Results indicate that for the specified location, the optimal orientation for maximizing energy yield is south, coupled with a tilt angle of 30°. This has consisted with the optimal tilt angle for Baghdad as presented in [1]. Interestingly, it's evident that the ideal tilt angle varies depending on the orientation of the modules.

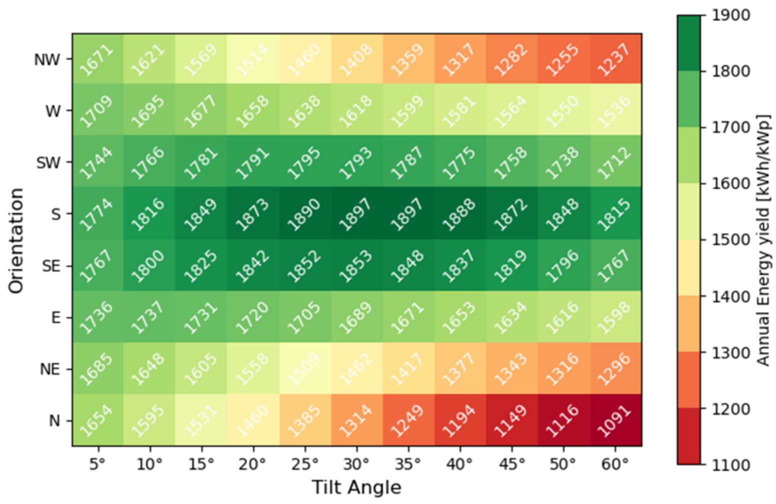

Orientation / Azimuth	Optimal tilt angle
NW: 315°	5°
West: 270°	5°
SW: 225°	25°
South: 180°	30°
SE: 135°	30°
East: 90°	10°
NE: 45°	5°
North: 0°	5°

Figure 7. (Left) is simulated annual energy yield at different orientations and tilt angles. (Right) is the table shows the optimal tilt angle at different orientations.

After determining the optimal tilt angle for each orientation based on the initial-year energy yield, we proceeded with a second assessment to understand the impact of orientation on climatic stressors and their implications for reliability, economics, and greenhouse gas emissions.

Figure 8 illustrates the Gpoa (A), module temperature (B) and power (C) for south-facing – 30° tilt and east-facing – 10° tilt PV modules simulated for an entire year in hourly resolution. From the figure its visible that there are differences in Gpoa, module temperature and power between south and east orientations. The differences in Gpoa are correlated with UV dose on an annual basis by using a simple linear estimation that UV dose is a 5% portion of the total annual irradiation as in [38]. Considering only south and east-facing modules, the evaluated degradation rates are 0.861%/year and 0.774%/year respectively. In Figure 8(D) the estimated degradation in energy yield for the south and east facing modules is shown. By defining the lifetime of the module as the 20% loss of the initial yield, the lifetime of the south-facing module is approximately 23 years compared to approximately 26 years for east-facing modules. It is noteworthy that the estimated degradation and lifetime of the modules exceed the current PV manufacturer's warranty of 0.45% per year or 30 years. This discrepancy is unsurprising given the harsh operating conditions, such as higher temperatures and irradiation, experienced by modules in Iraq. PV manufacturers often overlook climate-based warranties, and studies have shown significant variability in degradation rates based on climate [23], [52], [53]. Our recent analysis of two PV systems in Iraq revealed higher variations in degradation rates compared to the manufacturer's warranty [28]. In Figure 9 the annual UV dose and annual average module temperature for different azimuth/orientations are shown, further showing the energy yield during the first year (EY_Y1) and over the lifetime of the PV system (EY_LT) for different orientations. Also, the GHG emission factor changes with orientation since it varies with the energy yield and lifetime of the

PV system. Moreover, the financial parameters including CAPEX, OPEX and the LCOE are also presented.

It's worth noting that, for a fair comparison, we maintained the optimal tilt angle for each orientation when deriving other parameters. Additionally, please note that when evaluating EY_LT, the initial energy yield is consistent across all orientations and equals EY_Y1 at the optimal orientation. This uniformity arises because, in non-optimal orientations, additional modules are incorporated to achieve comparable energy output to that of the optimal orientation. This implies that the differences in the EY_LT are only related to the degradation and lifetime differences. Figure 10(A) depicts the pattern of the degradation rate regarding different installation orientations. It is visible that all the parameters are changing with the orientations. For example, the CAPEX increases as you shift from the south-facing orientation to other orientations mainly because you need additional modules and land surface to produce the same energy as shown in Figure 10(B).

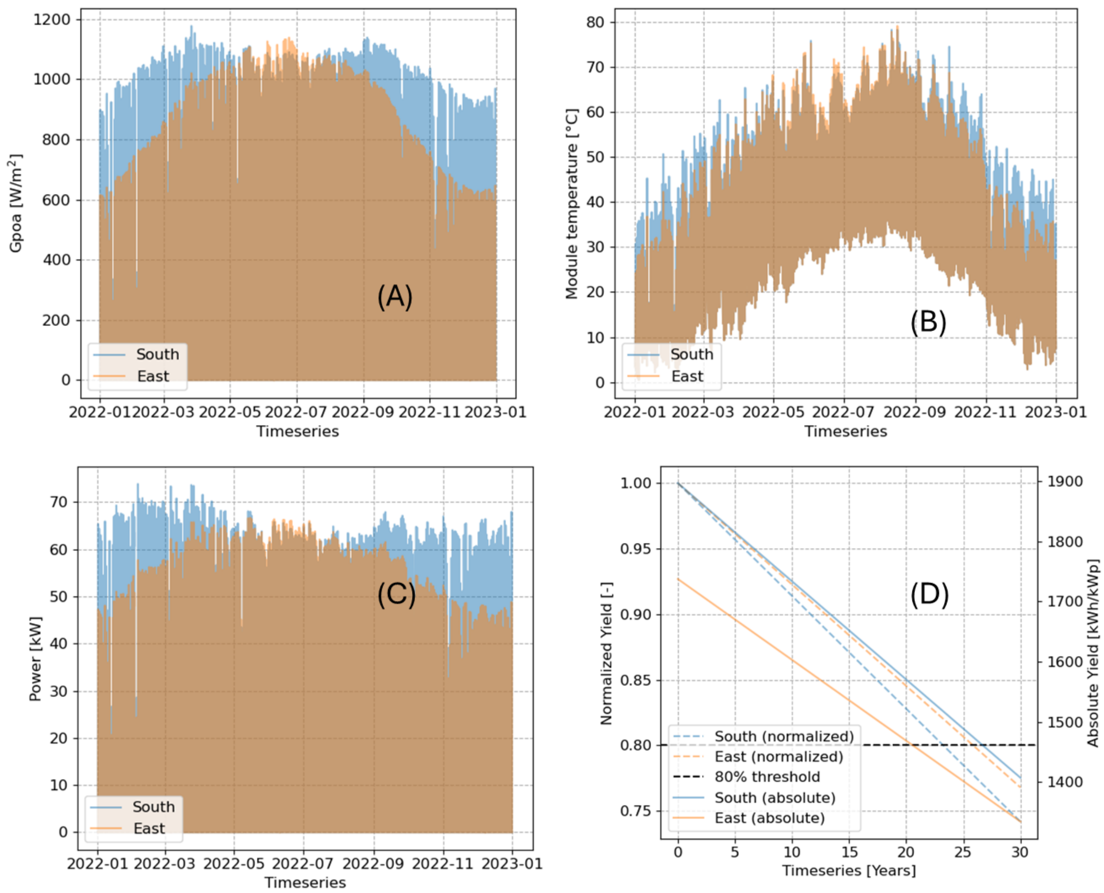

Figure 8. Simulated plane of array irradiance – Gpoa (A), Module temperature (B) and power (C) for south and east-facing PV systems. Figure (D) shows the energy yield degradation for south and east-facing systems corresponding to the differences in degradations due to different stress factors.

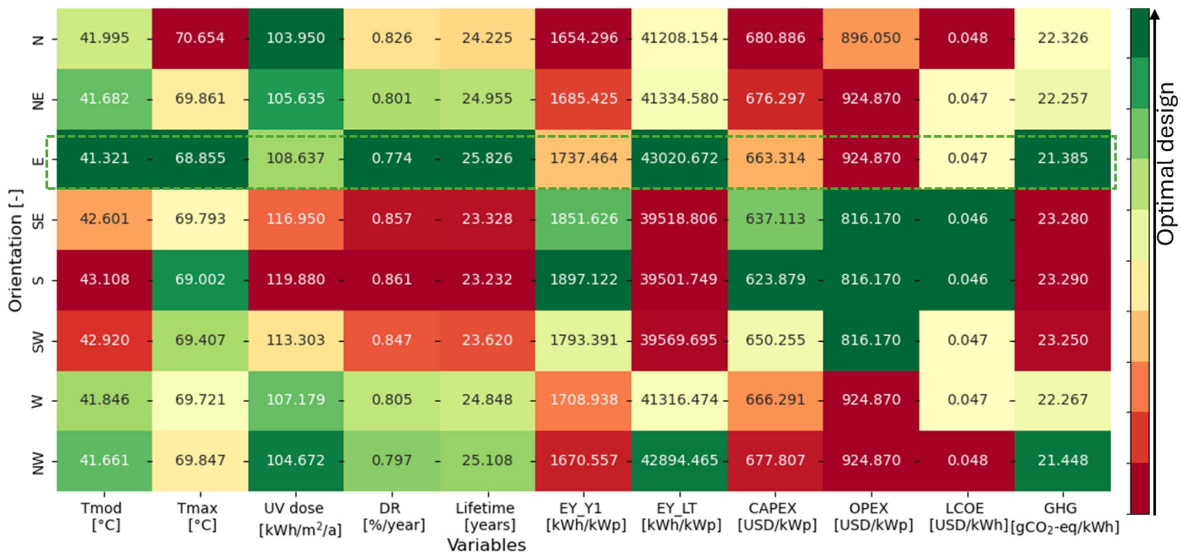

Figure 9. Simulated influence of orientation on climate stressors, degradation rate, energy yield, economic variables, and greenhouse gas emission factor. "EY_Y1" denotes the first-year energy yield without degradation, while "EY_LT" represents the lifetime energy yield considering degradation. (The optimal, indicated by the color bar, should ideally display a green hue across all variables)

Considering our threefold optimization strategy based on lifetime energy yield, LCOE, and GHG factors, east orientation emerges as the optimal choice since it provides the maximal lifetime energy yield and the lowest GHG emission despite its relatively higher LCOE compared to south and southeast orientations. When comparing module lifetimes across different orientations, the east orientation shows the longest PV module lifetime, while the south orientation has the shortest, with a difference of approximately three years. This extended lifetime for east orientation results in a positive gain in lifetime energy yield. However, the LCOE remains relatively higher for the east orientation compared to the south orientation. This indicates that the lifetime energy yield gain for east orientation does not offset the additional CAPEX and OPEX associated with east-oriented modules, thereby increasing the LCOE compared to south orientation.

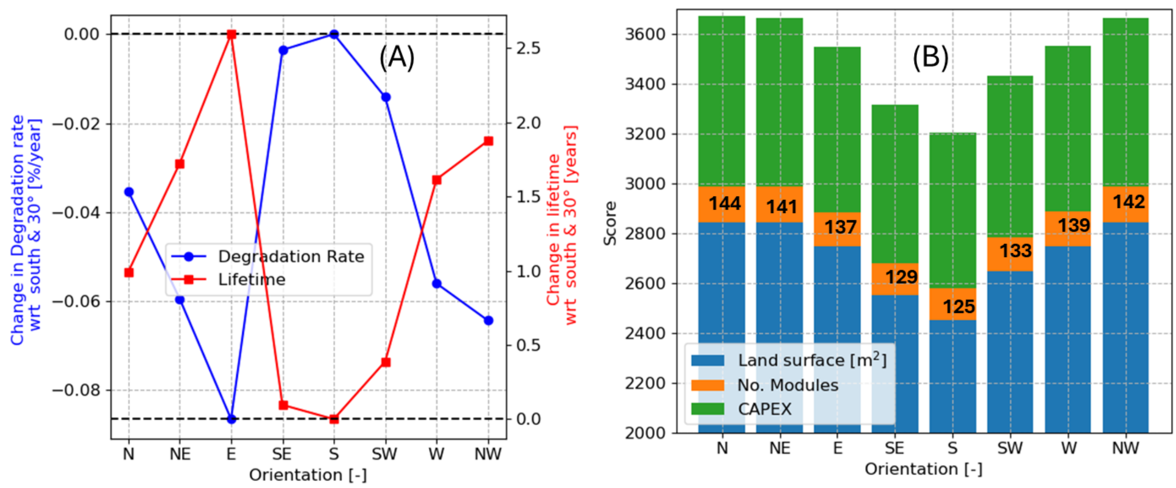

Figure 10. Simulated variations in degradation rate and lifetime in reference to the south (A) and (B) display stacked bar graphs depicting the necessary land surface, module count, and capital expenditure (CAPEX) across different orientations The values in the yellow segment indicate the required number of modules.

3.2 S2: Varied tilt angles at optimal azimuth

In this scenario, we conducted simulations to assess the optimal tilt angle based on lifetime energy yield, LCOE, and GHG factor. Throughout these simulations, the modules are orientated south, and the albedo, row pitch, and elevation of the modules remained constant at 0.20, 15.0 meters, and 2.0 meters, respectively. In Figure 11, the correlation between climate stressors (average module temperature Tmod, maximum module temperature Tmax, and UV dose) and the tilt angle is depicted, along with the degradation rate variations due to these stressors. The corresponding energy yield during the first year (EY_Y1) and over the PV system's lifetime (EY_LT) for different tilt angles is illustrated. Financial parameters such as CAPEX, lifetime OPEX and LCOE, as well as the greenhouse gas emission factor for each tilt angle, are also presented. Focusing solely on the first-year energy yield suggests that the optimum angle is 30° due to higher irradiation. However, considering the lifetime energy yield, LCOE, and GHG factor, the optimal tilt angle becomes 50°. Figure 12(A) depicts the pattern of the degradation rate regarding different installation tilted angles. Despite the higher initial yield at 30°, the elevated degradation rate and reduced lifetime diminish the overall lifetime energy yield compared to other tilt angles. It is noteworthy that CAPEX rises for alternative tilt angles compared to 30° since the energy yield for these angles is normalized to that of 30°, necessitating more modules, land, and installation structures, consequently increasing the CAPEX as shown in Figure 12(B). Additionally, steeper tilt angles can increase substructure costs due to the need for more steel, raising the CAPEX. For simplicity, we assumed similar substructures for all tilt angles in this study, but our methodology allows for the inclusion of extra structural costs if known. The lifetime OPEX increases with an increase in the lifetime of the PV system since extra operational costs are needed for these extra operational years.

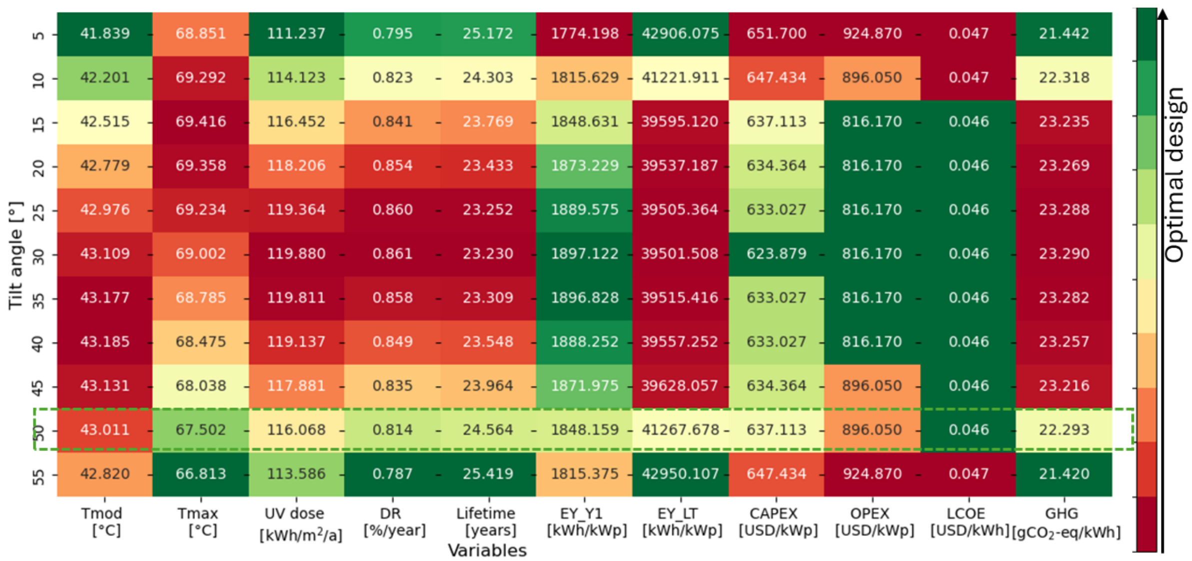

Figure 11. Simulated influence of tilt angle on climate stressors, degradation rate, energy yield, economic variables, and greenhouse gas emission factor. "EY_Y1" denotes the first-year energy yield without degradation, while "EY_LT" represents the lifetime energy yield considering degradation.

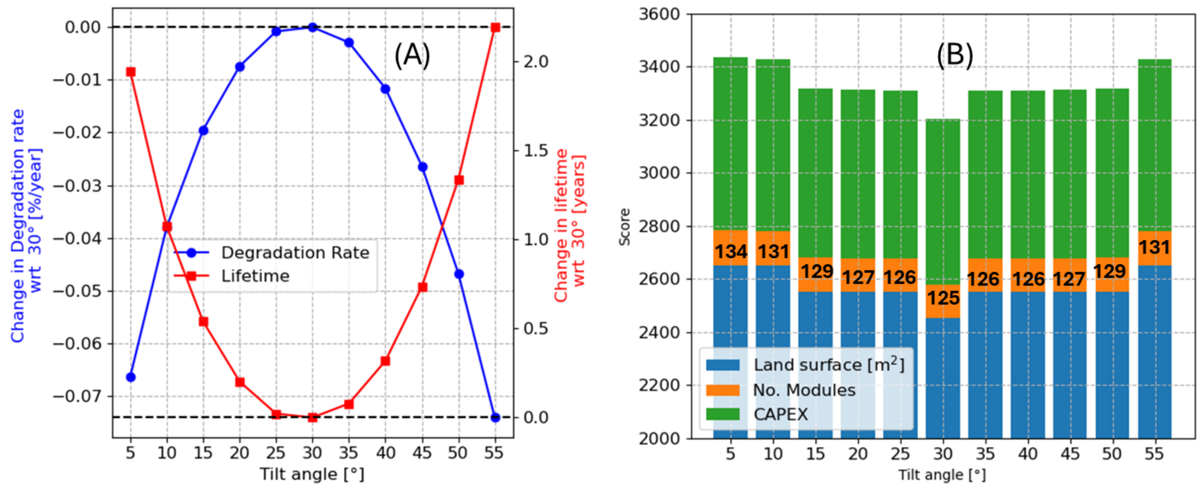

Figure 12. Simulated variations in degradation rate and lifetime in reference to tilt angle of 30° (A). Stacked bar graphs depicting the necessary land surface, module count, and capital expenditure (CAPEX) across different tilt angles (B). The values in the yellow segment indicate the required number of modules.

To further investigate the advantages of opting for a tilt angle of 50° over 30° in our system installation, we examined the impact of tilt angle on soiling accumulation. Figure 13(A) presents the simulated soiling ratio at various tilt angles, considering only natural cleaning by rainfall, with a cleaning threshold set at 5mm of daily rainfall accumulation. In Figure 13(B), it is evident that with an increasing tilt angle, the annual energy yield loss attributed to soiling diminishes, affirming the suitability of installing PV modules at a 50° tilt angle in this location.

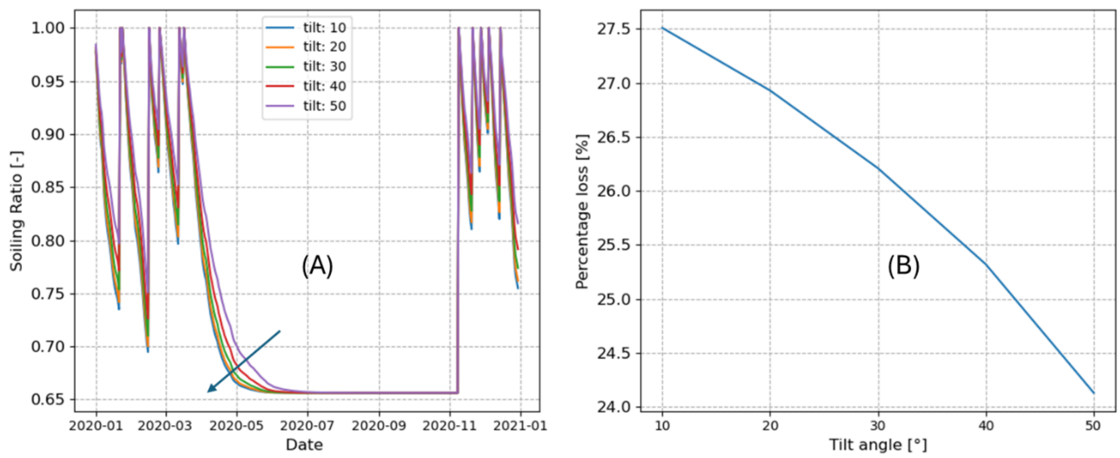

Figure 13. Simulated soiling ratio for different tilt angles (A) and simulated annual energy yield loss at different tilt angles in Baghdad (B).

3.3 S3: Varied row pitch at optimal tilt angle and azimuth

In this scenario, we conducted simulations to assess the optimal row pitch based on lifetime energy yield, LCOE, and GHG factor. Throughout these simulations, the modules are orientated south, and the tilt angle, albedo, and elevation of the modules remained constant at 30°, 0.40, and 1.0 meters, respectively. More specifically, the correlation between row pitch and energy yield is depicted in column EY_Y1 in Figure 14. As expected, energy yield increases with increasing row pitch which is related to reduced row-to-row shading compared to smaller row pitches. However, larger pitches require more land area and can increase installation costs as illustrated in Figure 15(B).

PV system installed with a 5m row pitch gains a 1.3-year lifetime as compared to a PV system installed with a 30m row pitch as shown in Figure 15(A). This extra gain in lifetime improves the systems' lifetime energy yield (EY_LT) by approximately 4.3%. This gain in EY_LT coupled with reduced CAPEX lowers the LCOE and the GHG emission factors hence making 5 m the optimal row pitch. However, it is important to note that very short row pitch can cause significant row-to-row shading, which may result in hot spots and further long-term degradation. Unfortunately, current degradation models are not capable of accurately modelling the complex relationship between shading, hot spots, and their impact on long-term degradation rates.

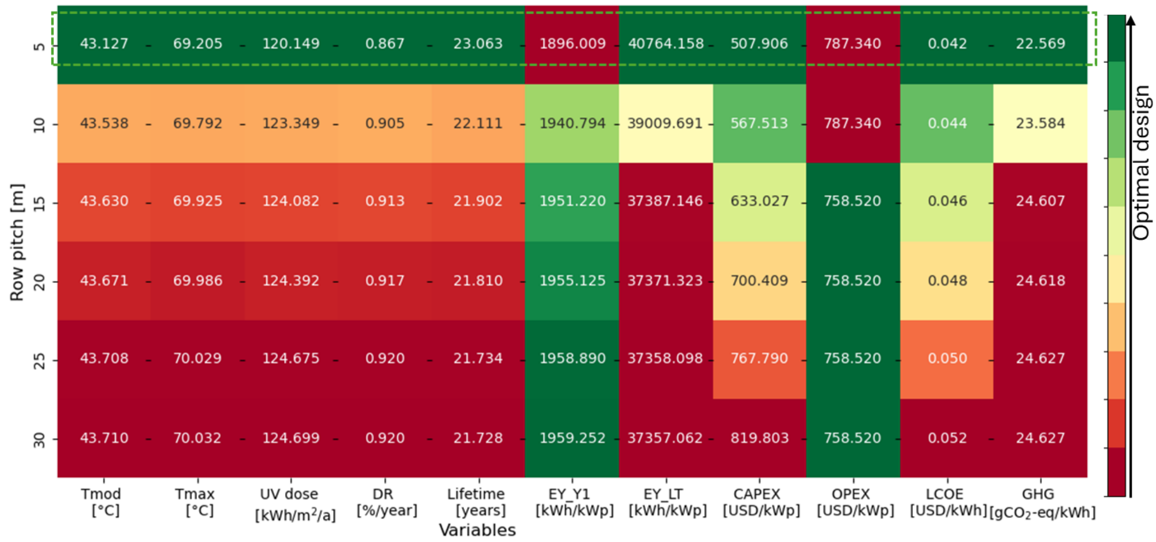

Figure 14. Simulated influence of row pitch on climate stressors, degradation rate, energy yield, economic variables, and greenhouse gas emission factor. "EY_Y1" denotes the first-year energy yield without degradation, while "EY_LT" represents the lifetime energy yield considering degradation.

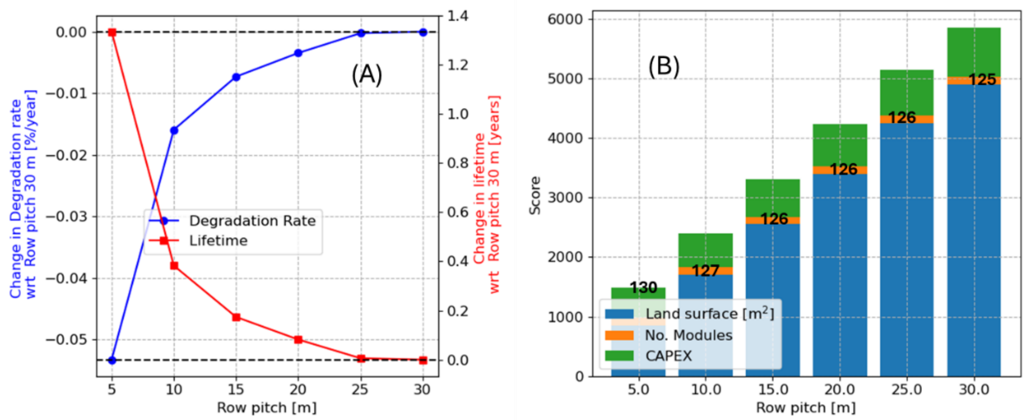

Figure 15. Simulated variations in degradation rate and lifetime in reference to row pitch of 30m (A) and (B) display stacked bar graphs depicting the necessary land surface, module count, and capital expenditure (CAPEX) across different row pitches the values in the yellow segment indicate the required number of modules.

3.4 S4: Varied PV system elevated height at optimal tilt angle and azimuth

The impact of PV system elevation was simulated at heights ranging from 0.5m to 3m, with a fixed tilt angle of 30°, row pitch of 10m, albedo of 0.4, and a south-facing orientation. Figure 16 illustrates the simulated performance, financial, and GHG emission parameters at various system heights. It is evident that energy yield (EY_YI) increases with greater elevation. This is especially true for bifacial modules, where elevation enhances rear-side irradiance. Modules installed at higher elevations capture more diffuse irradiance compared to those at lower heights. Additionally, increased height is necessary to minimize the effects of shadowing and to provide a broader field view of the unshaded ground [2].

Some studies have indicated that higher elevation leads to better convective cooling, resulting in lower operating temperatures and increased energy yields [54]. However, other research has found that the higher irradiance on elevated PV arrays increases module temperatures, counteracting the benefits of convective cooling [55]. This latter finding aligns with our simulation, which shows that modules installed at higher elevations operate at higher temperatures due to increased irradiance. Consequently, the combination of higher operating temperatures and increased irradiance at higher elevations negatively impacts the degradation rate and lifetime of the PV modules.

In Figure 17(A) we observe that modules installed at a height of 0.5-meter have an approximately 4.0-year longer lifetime compared to those installed at 3 meters. This increased lifetime for the 0.5-meter modules results in a higher lifetime energy yield compared to the 3-meter modules. Furthermore, Figure 17(B) indicates that while modules installed at 3 meters require less land surface to produce the same amount of energy, the additional installation structure costs make the total CAPEX higher for modules at 3 meters. Conversely, the lifetime OPEX is higher for the 0.5-meter modules due to the additional operational costs incurred over the extra 4.0 years of lifetime. Overall, considering the three main indicators EY_LT, LCOE, and GHG emission factor, the optimal installation height would be 0.5 meters. However, we suggested selecting 1.0-meter as optimal considering that more OPEX is required for 0.5 meter in comparison to 1.0-meter and both heights have similar LCOEs and the difference in GHG emission factor is negligible. Additionally, considering other reliability factors such as wind load damage, further supports the conclusion that installing a PV system at a lower elevation is more advantageous.

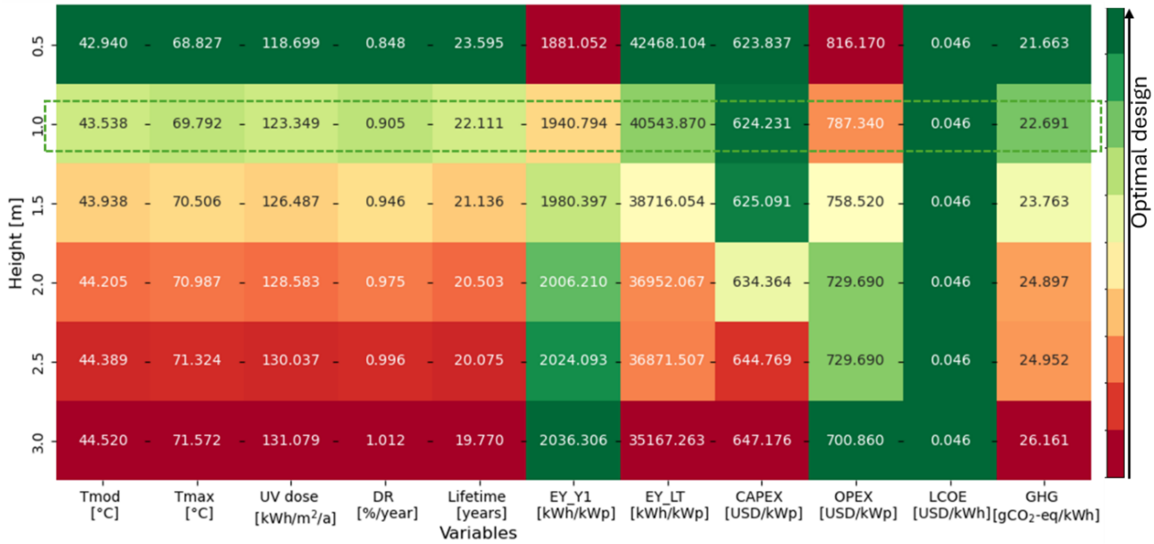

Figure 16. Simulated influence of installation height on climate stressors, degradation rate, energy yield, economic variables, and greenhouse gas emission factor. "EY_Y1" denotes the first-year energy yield without degradation, while "EY_LT" represents the lifetime energy yield considering degradation.

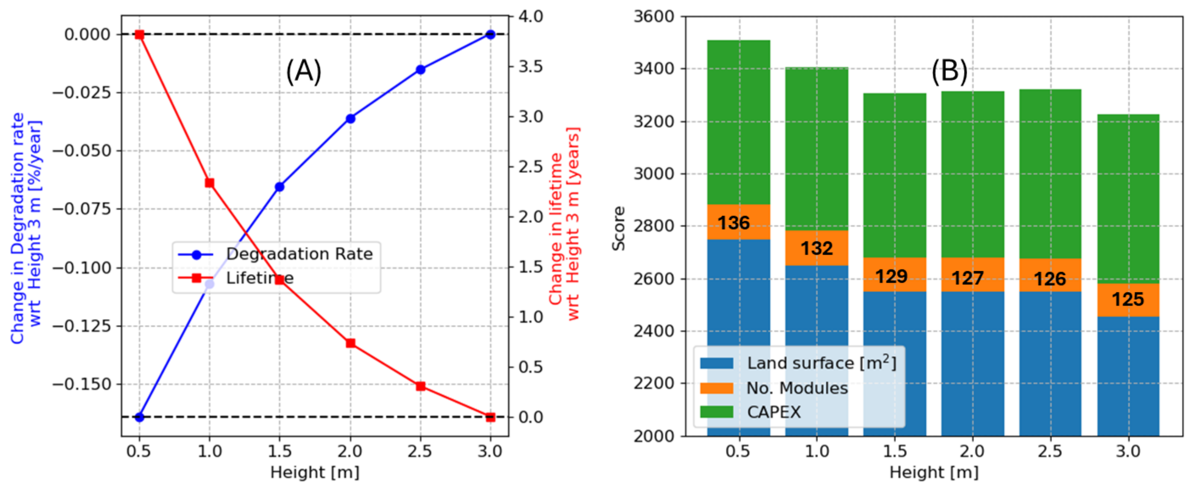

Figure 17. Simulated variations in degradation rate and lifetime in reference to height of 4m (A) and (B) display stacked bar graphs depicting the necessary land surface, module count, and capital expenditure (CAPEX) across different heights The values in the yellow segment indicate the required number of modules.

3.5 S5: Varied albedo at optimal tilt angle and azimuth

Higher ground albedo results in increased reflectance, which enhances the rear side irradiance of bifacial modules. Studies and simulations have demonstrated that as ground albedo increases, the energy gain from bifacial modules also rises[56], [57]. This is because the rear side of the modules can absorb more reflected light, effectively converting it into additional electrical energy. The impact of albedo on irradiance and energy gain is well documented but the subsequent impact on operating module temperature has not been studied to the best of our knowledge. In this study, we were interested in accessing through simulation and experiment how the albedo impacts the operating temperature of the PV modules. We hypothesise that modules operating at higher irradiance in our case with higher albedo increase module temperatures as well.

Figure 18(A) shows the average measured albedo for the white fabric, desert sand, and grass fabric during the testing period. The histogram in Figure 18(B) displays the corresponding measured temperatures of the three ground surfaces during the testing period. A close examination of the temperature profiles reveals that the white polymer operates at a maximum temperature of 66.0°C, which is relatively higher compared to sand at 65.9°C and grass fabric at 64.5°C. Note that this experiment was conducted over a short period as a proof of concept. To assess the long-term impact, including seasonal effects, we provide a full-year simulation at different effective albedo levels of 0.25, 0.33, and 0.49 corresponding to those measured for grass fabric, sand and white fabric respectively as per Figure 18(C). The maximum operating temperatures at these albedo levels are evaluated as 77.8°C, 78.5°C, and 79.9°C, respectively. This is consistent with our measurements and hypothesis that module operating temperatures increase with rising albedo.

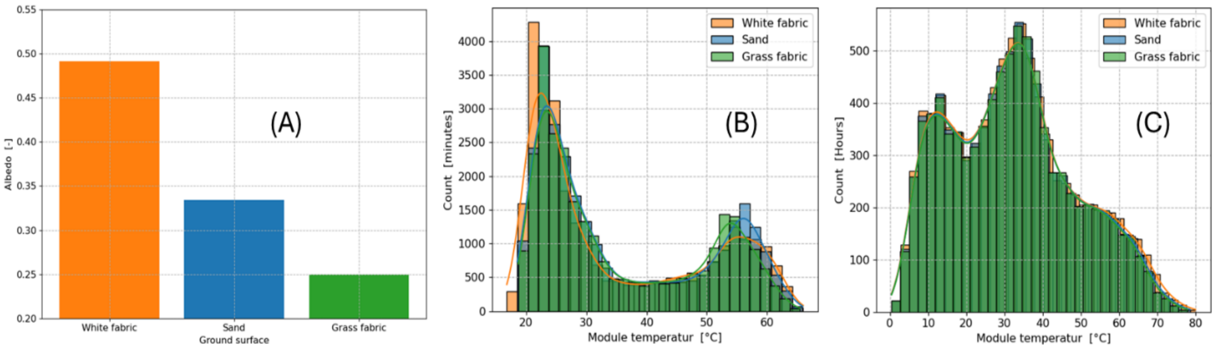

Figure 18. Mean measured albedo for different ground surfaces during the testing period (A), measured module temperature histograms during the testing period for different ground surfaces with ±1.0°C (B) and simulated module temperature histograms for a period of one year (C) for different albedo values.

Figure 19 provides a comprehensive overview of the impact of albedo on stress factors, degradation rate, energy yield, financial parameters, and GHG emissions. It demonstrates that the albedo significantly affects stress factors, which in turn have a substantial impact on the degradation rate and PV lifetime. Figure 20(A) shows that the lifetime difference exceeds 8 years when comparing albedos of 0.1 and 0.9. This difference in lifetime affects the lifetime energy yield, greenhouse gas emission factor, and financial parameters such as CAPEX (see Figure 20(B)) and OPEX.

In selecting the albedo based on our threefold approach, an albedo of 0.1 provides the highest lifetime energy yield and the lowest GHG emissions factor but also has the highest LCOE. Conversely, an albedo of 0.9 results in the lowest LCOE but the highest GHG emissions and the lowest lifetime energy yield. Therefore, the best choice, considering all three indicators, is an albedo of 0.5, despite its higher GHG emissions compared to albedo of 0.1 and 0.3. This is an exciting result because the best-simulated albedo matches the measured albedo for desert sand, suggesting that if the goal is to optimize not only the LCOE but also GHG emissions, applying albedo boosters may not be necessary in desert climates. Furthermore, the cost of boosters was not included in the calculations, which could potentially match the LCOE of 0.9 with that of 0.5 if included hence confirming that no need for albedo boosters in desert climates.

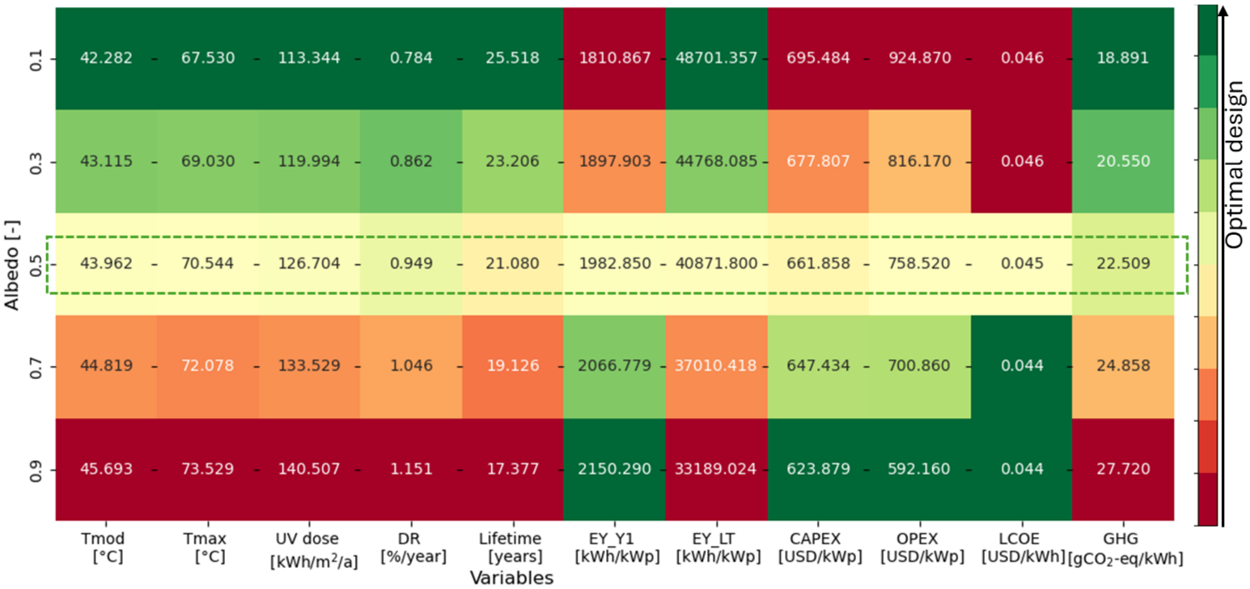

Figure 19. Simulated influence of ground albedo on climate stressors, degradation rate, energy yield, economic variables, and greenhouse gas emission factor. "EY_Y1" denotes the first-year energy yield without degradation, while "EY_LT" represents the lifetime energy yield considering degradation.

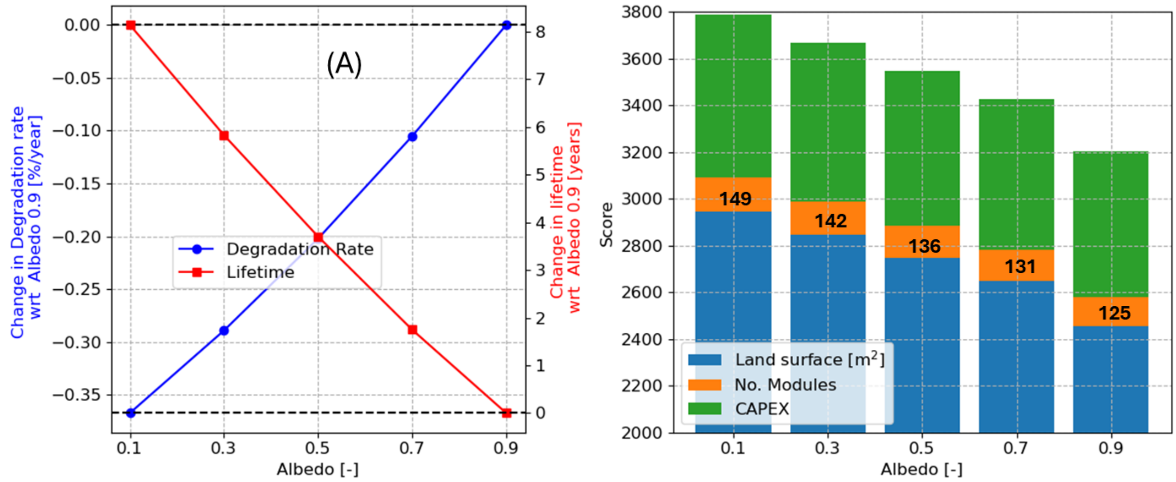

Figure 20. Simulated variations in degradation rate and lifetime in reference to albedo of 0.9 (A) and (B) display stacked bar graphs depicting the necessary land surface, module count, and capital expenditure (CAPEX) across different albedos. The values in the yellow segment indicate the required number of modules.

3.6 Highlight of all the scenarios

Table 5 summarizes the impact of installation parameters on PV module lifetime, lifetime energy yield, LCOE, and GHG emissions. The percentage change is calculated using Equation Eq.(10). We benchmark the installation parameters that cause the maximum variation against the scenario that yields the highest energy output (EY_Y1 – the standard definition of optimal installation).

Excluding albedo initially, system elevation exhibits the highest sensitivity compared to tilt angle, azimuth, and row pitch, showing the greatest percentage change in lifetime, energy yield, and GHG emissions due to bifaciality effects. When albedo is considered, it has the most significant influence on all aspects of reliability, performance, financial metrics, and GHG emissions. It should be noted that the results presented here are highly dependent on the specific location and the assumptions used in parameterizing the degradation rate model. The impact of UV due to albedo might be minimal when using PV modules with low sensitivity to UV degradation. However, higher albedo can lead to differences in operating temperatures, which may influence other degradation mechanisms.

The LCOE variation is not substantial in most scenarios compared to other variables such as lifetime yield and GHG emissions. This is because, with the installation parameter-based degradation rates approach proposed in this study, some variables affecting LCOE offset each other. For instance, higher OPEX and CAPEX in given scenario can be balanced by a higher lifetime yield, resulting in relatively stable LCOE across most scenarios.

Table 5. Maximum /percentage change in lifetime, lifetime yield, LCOE and GHG emission factor for the simulated installation parameters. (Hint: Higher values for lifetime and lifetime yield are preferable, while lower values for LCOE and GHG emissions are desirable - the negative values for LCOE and GHG represent good case scenarios since we aim to lower these variables)

Installation parameter	**Maximum / Percentage change**			
	lifetime [years]	Lifetime yield	LCOE	GHG emission
Azimuth	2.6	8.90%	4.35%	-8.30%
Tilt angle	2.2	8.70%	2.17%	-8.00%
Row pitch	1.4	9.10%	-19.23%	-8.40%
Elevation	3.8	20.80%	0.00%	-17.20%
Albedo	8.1	46.74%	4.55%	-38.85%

3.7 Study applicability and limitations

This section discusses both the potential applications and limitations of the study's findings, aiming to guide future research directions and the possibility of reproducing the results.

In terms of applicability and reproducibility, our study primarily aimed to challenge the current practice of relying solely on the LCOE based on first-year energy yield for determining optimal installation parameters. Instead, we introduced a threefold optimization strategy that integrates additional indicators such as lifetime energy yield and GHG emission factors. We outlined a methodology and provided a case study to illustrate how this approach could be implemented. Various tools and models exist for estimating energy yield, degradation rates, LCOE, and environmental impacts. In our study, we selected tools based on literature and, in some cases, utilized simplified versions of these models. Importantly, our methodology is adaptable; if more accurate tools or models become available, they can be substituted within the optimization strategy.

However, the study has several limitations. Our findings are influenced by specific geographic locations and assumptions inherent in the models used. Input parameters, particularly for degradation models (technology-specific) and financial models (e.g., land prices, structure costs), as well as GHG models (e.g., emissions during transportation and installation), are influenced by location and time. Many of these parameters were approximated based on literature values, which may not precisely reflect the most recent or future conditions. Consequently, LCOE and GHG emission factors may vary over time and locations.

It's essential to clarify that our study does not claim the universal applicability of the optimal parameters identified. Rather, our primary objective is to present a methodology that enables the evaluation of optimal parameters based on specific considerations relevant to installers. This study serves as a case example, recognizing that outcomes can vary based on the specific factors evaluated.

4. Conclusion

The study explores, the influence of different PV system designs on the climate stressors that is module temperature and solar irradiation and how this influences the lifetime of the PV modules, especially in harsh climates like Iraq. We used a physics-based energy yield simulation framework, and a physics-based degradation model to evaluate these variations in lifetime due to installation parameters. In the study, a novel optimization strategy for PV systems is proposed, which considers three indicators: lifetime energy yield, LCOE, and GHG emission factors, rather than solely economic aspects as is common practice.

Our simulations demonstrated that a 50° tilt angle for PV modules, though initially costlier, maximizes lifetime energy yield, minimizes LCOE, and reduces GHG emissions compared to a 30° tilt angle. This optimal tilt angle also decreases energy losses due to soiling.

Our findings show that a PV system with a 5-meter row pitch gains an additional 1.3 years of lifetime compared to one with a 30-meter row pitch, enhancing the lifetime energy yield by approximately 4.3%. This increase in lifetime energy yield, along with reduced CAPEX, lowers the LCOE and GHG emission factors, making 5-meters the optimal row pitch for PV installation in the studied scenario.

Our study found that PV modules installed at a height of 0.5-meter have a longer lifetime and higher energy yield but incur higher operational costs. Considering overall performance and reliability, we recommend an optimal installation height of 1.0-meter for balancing cost, performance, and environmental impact.

We showed that albedo significantly influences PV module degradation rates, lifetime energy yield, and financial parameters. While an albedo of 0.1 offers the highest energy yield and lowest GHG emissions, it results in the highest LCOE. Conversely, an albedo of 0.9 has the lowest LCOE but the highest GHG emissions and lowest energy yield. An albedo of 0.5 provides the best balance among these factors. This finding is particularly relevant for desert climates, where in some cases natural albedo matches this optimal value, indicating that albedo boosters might be unnecessary.

The study emphasizes that optimal design should not be determined solely by the first-year energy yield but should consider factors such as lifetime energy yield, LCOE, and GHG emissions. Further and ongoing work is to propose an indoor accelerated experiment that can help to simulate the effect of tilt angle on PV lifetime in a short time to validate the reliability models.

Reference

[1] M. Z. Jacobson and V. Jadhav, "World estimates of PV optimal tilt angles and ratios of sunlight incident upon tilted and tracked PV panels relative to horizontal panels," *Solar Energy*, vol. 169, pp. 55–66, Jul. 2018, doi: 10.1016/j.solener.2018.04.030.

[2] A. Asgharzadeh, B. Marion, C. Deline, C. Hansen, J. S. Stein, and F. Toor, "A Sensitivity Study of the Impact of Installation Parameters and System Configuration on the Performance of Bifacial PV Arrays," *IEEE Journal of Photovoltaics*, vol. 8, no. 3, pp. 798–805, May 2018, doi: 10.1109/JPHOTOV.2018.2819676.

[3] D. Berrian and J. Linder, "Enhanced Bifacial Gain with Optimized Mountings in Photovoltaic Systems," *Solar RRL*, vol. 7, no. 23, p. 2300474, 2023, doi: 10.1002/solr.202300474.

[4] R. Arena, S. Aneli, A. Gagliano, and G. M. Tina, "Optimal Photovoltaic Array Layout of Agrivoltaic Systems Based on Vertical Bifacial Photovoltaic Modules," *Solar RRL*, vol. 8, no. 1, p. 2300505, 2024, doi: 10.1002/solr.202300505.

[5] R. Abdallah, A. Juaidi, S. Abdel-Fattah, and F. Manzano-Agugliaro, "Estimating the Optimum Tilt Angles for South-Facing Surfaces in Palestine," *Energies*, vol. 13, no. 3, Art. no. 3, Jan. 2020, doi: 10.3390/en13030623.

[6] C. Yu, Y. S. Khoo, J. Chai, S. Han, and J. Yao, "Optimal Orientation and Tilt Angle for Maximizing in-Plane Solar Irradiation for PV Applications in Japan," *Sustainability*, vol. 11, no. 7, Art. no. 7, Jan. 2019, doi: 10.3390/su11072016.

[7] H. Z. Al Garni, A. Awasthi, and D. Wright, "Optimal orientation angles for maximizing energy yield for solar PV in Saudi Arabia," *Renewable Energy*, vol. 133, pp. 538–550, Apr. 2019, doi: 10.1016/j.renene.2018.10.048.

[8] R. B. Mansour, M. A. Mateen Khan, F. A. Alsulaiman, and R. B. Mansour, "Optimizing the Solar PV Tilt Angle to Maximize the Power Output: A Case Study for Saudi Arabia," *IEEE Access*, vol. 9, pp. 15914–15928, 2021, doi: 10.1109/ACCESS.2021.3052933.

[9] F. Fertig *et al.*, "Mass production of *p*-type Cz silicon solar cells approaching average stable conversion efficiencies of 22 %," *Energy Procedia*, vol. 124, pp. 338–345, Sep. 2017, doi: 10.1016/j.egypro.2017.09.308.

[10] A. Sinha *et al.*, "UV-induced degradation of high-efficiency silicon PV modules with different cell architectures," *Progress in Photovoltaics: Research and Applications*, vol. 31, no. 1, pp. 36–51, 2023, doi: 10.1002/pip.3606.

[11] R. Witteck *et al.*, “UV radiation hardness of photovoltaic modules featuring crystalline Si solar cells with AlO_x /p $^+$ -type Si and SiN_y /n $^+$ -type Si interfaces,” *Physica Rapid Research Ltrs*, vol. 11, no. 8, p. 1700178, Aug. 2017, doi: 10.1002/pssr.201700178.

[12] K. Ilse *et al.*, “Techno-Economic Assessment of Soiling Losses and Mitigation Strategies for Solar Power Generation,” *Joule*, vol. 3, no. 10, pp. 2303–2321, Oct. 2019, doi: 10.1016/j.joule.2019.08.019.

[13] Y. A. Badamasi, S. Oodo, N. B. Gafai, and F. B. Ilyasu, “Effect of Tilt Angle and Soiling on Photovoltaic Modules Losses,” in *2021 1st International Conference on Multidisciplinary Engineering and Applied Science (ICMEAS)*, Jul. 2021, pp. 1–5. doi: 10.1109/ICMEAS52683.2021.9692375.

[14] A. Ullah, H. Imran, Z. Maqsood, and N. Z. Butt, “Investigation of optimal tilt angles and effects of soiling on PV energy production in Pakistan,” *Renewable Energy*, vol. 139, pp. 830–843, Aug. 2019, doi: 10.1016/j.renene.2019.02.114.

[15] J. Cano, G. Tamizhmani, C. Madakannan, and N. Macia, “Photovoltaic Modules: Effect of Tilt Angle on Soiling,” *2014 IEEE 40th Photovoltaic Specialist Conference, PVSC 2014*, Jun. 2014, doi: 10.1109/PVSC.2014.6925610.

[16] B. Figgis, D. Goossens, B. Guo, and K. Ilse, “Effect of tilt angle on soiling in perpendicular wind,” *Solar Energy*, vol. 194, pp. 294–301, Dec. 2019, doi: 10.1016/j.solener.2019.10.062.

[17] S. Bouguerra, K. Agroui, I. Kaaya, A. Bouraiou, M. R. Yaiche, and D. E. Mansour, “Modeling the Effect of PV Module Orientation on the Encapsulant Browning Degradation Rate in Algeria Region,” *IEEE Journal of Photovoltaics*, vol. 12, no. 1, pp. 274–284, Jan. 2022, doi: 10.1109/JPHOTOV.2021.3124749.

[18] L. J. Piotrowski and F. A. Farret, “Feasibility of solar tracking and fixed topologies considering the estimated degradation and performance of photovoltaic panels,” *Solar Energy Materials and Solar Cells*, vol. 244, p. 111834, Aug. 2022, doi: 10.1016/j.solmat.2022.111834.

[19] B. Adothu *et al.*, “Identification and Investigation of Materials Degradation in Photovoltaic Modules from Middle East Hot Desert,” p. 574 kB, 4 pages, doi: 10.4229/EUPVSEC2023/3AV.2.29.

[20] M. Mehdi, N. Ammari, A. Alami Merrouni, H. El Gallassi, M. Dahmani, and A. Ghennioui, “An experimental comparative analysis of different PV technologies performance including the influence of hot-arid climatic parameters: Toward a realistic yield assessment for desert locations,” *Renewable Energy*, vol. 205, pp. 695–716, Mar. 2023, doi: 10.1016/j.renene.2023.01.082.

[21] I. T. Horváth *et al.*, “Photovoltaic energy yield modelling under desert and moderate climates: What-if exploration of different cell technologies,” *Solar Energy*, vol. 173, pp. 728–739, Oct. 2018, doi: 10.1016/j.solener.2018.07.079.

[22] R. R. Cordero *et al.*, “Effects of soiling on photovoltaic (PV) modules in the Atacama Desert,” *Sci Rep*, vol. 8, no. 1, Art. no. 1, Sep. 2018, doi: 10.1038/s41598-018-32291-8.

[23] D. C. Jordan, S. R. Kurtz, K. VanSant, and J. Newmiller, “Compendium of photovoltaic degradation rates,” *Progress in Photovoltaics: Research and Applications*, vol. 24, no. 7, pp. 978–989, 2016, doi: 10.1002/pip.2744.

[24] D. Hassan Daher, L. Gaillard, and C. Ménézo, “Experimental assessment of long-term performance degradation for a PV power plant operating in a desert maritime climate,” *Renewable Energy*, vol. 187, pp. 44–55, Mar. 2022, doi: 10.1016/j.renene.2022.01.056.

[25] X. Huang, H. Wang, X. Jiang, and H. Yang, “Performance degradation and reliability evaluation of crystalline silicon photovoltaic modules without and with considering measurement reproducibility: A case study in desert area,” *Renewable Energy*, vol. 219, p. 119421, Dec. 2023, doi: 10.1016/j.renene.2023.119421.

[26] A. Bouraiou *et al.*, “Analysis and evaluation of the impact of climatic conditions on the photovoltaic modules performance in the desert environment,” *Energy Conversion and Management*, vol. 106, pp. 1345–1355, Dec. 2015, doi: 10.1016/j.enconman.2015.10.073.

[27] A. Necaibia *et al.*, "Analytical assessment of the outdoor performance and efficiency of the grid-tied photovoltaic system under hot dry climate in the south of Algeria," *Energy Conversion and Management*, vol. 171, pp. 778–786, Sep. 2018, doi: 10.1016/j.enconman.2018.06.020.
[28] M. A. Hameed, I. Kaaya, M. Al-Jbori, Q. Matti, R. Scheer, and R. Gottschalg, "Analysis and Prediction of the Performance and Reliability of PV Modules installed in harsh climates: Case study Iraq," *Renewable Energy*, p. 120577, Apr. 2024, doi: 10.1016/j.renene.2024.120577.
[29] J.-F. Lelièvre *et al.*, "Desert label development for improved reliability and durability of photovoltaic modules in harsh desert conditions," *Solar Energy Materials and Solar Cells*, vol. 236, p. 111508, Mar. 2022, doi: 10.1016/j.solmat.2021.111508.
[30] I. Horvath *et al.*, *Next Generation Tools for Accurate Energy Yield Estimation of Bifacial PV Systems – Best Practices, Improvements and Challenges*. 2019.
[31] H. Goverde, F. Catthoor, V. Dubey, and C. BAERT, "SIMULATION OF PHOTOVOLTAIC MODULES." Accessed: Dec. 15, 2023. [Online]. Available: https://data.epo.org/publication-server/document?iDocId=5026454&iFormat=0
[32] F. Catthoor, M.-I. BAKA, and P. MANGANIELLO, "SIMULATION OF PHOTOVOLTAIC SYSTEMS." Accessed: Dec. 15, 2023. [Online]. Available: https://data.epo.org/publication-server/document?iDocId=5026454&iFormat=0
[33] I. Kaaya, M. Köhl, A. Mehilli, S. de C. Mariano, and K. A. Weiss, "Modeling Outdoor Service Lifetime Prediction of PV Modules: Effects of Combined Climatic Stressors on PV Module Power Degradation," *IEEE Journal of Photovoltaics*, vol. 9, pp. 1105–1112, 2019, doi: 10.1002/pip.2793.
[34] I. Kaaya, D. Mansour, P. Gebhardt, K. Weiß, and D. Philipp, "Modelling and Validation of Photovoltaic Degradation under Ultraviolet-Damp-Heat Conditions," *2021 IEEE 48th Photovoltaic Specialists Conference (PVSC)*, 2021, doi: 10.1109/PVSC43889.2021.9519050.
[35] I. Kaaya, J. Ascencio-Vásquez, K.-A. Weiss, and M. Topič, "Assessment of uncertainties and variations in PV modules degradation rates and lifetime predictions using physical models," *Solar Energy*, vol. 218, pp. 354–367, Apr. 2021, doi: 10.1016/j.solener.2021.01.071.
[36] "scipy.stats.ncf — SciPy v1.11.1 Manual." Accessed: Jul. 05, 2023. [Online]. Available: https://docs.scipy.org/doc/scipy/reference/generated/scipy.stats.ncf.html
[37] S. Lindig, I. Kaaya, K.-A. Weiß, D. Moser, and M. Topic, "Review of Statistical and Analytical Degradation Models for Photovoltaic Modules and Systems as Well as Related Improvements," *IEEE Journal of Photovoltaics*, vol. 8, no. 6, pp. 1773–1786, Nov. 2018, doi: 10.1109/JPHOTOV.2018.2870532.
[38] M. Koehl, M. Heck, and S. Wiesmeier, "Categorization of weathering stresses for photovoltaic modules," *Energy Science & Engineering*, vol. 6, no. 2, pp. 93–111, 2018, doi: 10.1002/ese3.189.
[39] A. Louwen, R. E. I. Schropp, W. G. J. H. M. van Sark, and A. P. C. Faaij, "Geospatial analysis of the energy yield and environmental footprint of different photovoltaic module technologies," *Solar Energy*, vol. 155, pp. 1339–1353, Oct. 2017, doi: 10.1016/j.solener.2017.07.056.
[40] A. Müller, L. Friedrich, C. Reichel, S. Herceg, M. Mittag, and D. H. Neuhaus, "A comparative life cycle assessment of silicon PV modules: Impact of module design, manufacturing location and inventory," *Solar Energy Materials and Solar Cells*, vol. 230, p. 111277, Sep. 2021, doi: 10.1016/j.solmat.2021.111277.
[41] S. Krauter and R. Rüther, "Considerations for the calculation of greenhouse gas reduction by photovoltaic solar energy," *Renewable Energy*, vol. 29, no. 3, pp. 345–355, Mar. 2004, doi: 10.1016/S0960-1481(03)00251-9.
[42] E. A. Alsema and M. J. de Wild, "Environmental Impacts of Crystalline Silicon Photovoltaic Module Production," *MRS Online Proceedings Library*, vol. 895, no. 1, p. 305, Apr. 2006, doi: 10.1557/PROC-0895-G03-05.
[43] C. Tjengdrawira, "Best Practice Guidelines for PV Cost Calculation, Accounting for Technical Risks and Assumptions in PV LCOE".

[44] M. A. Hameed, D. Daßler, Q. M. Alias, R. Scheer, and R. Gottschalg, "Economic Consequences Based on Reversible and Irreversible Degradation of PV Park in the Harsh Climate Conditions of Iraq," *Energies*, vol. 17, no. 11, Art. no. 11, Jan. 2024, doi: 10.3390/en17112652.
[45] "JRC Photovoltaic Geographical Information System (PVGIS) - European Commission." Accessed: Apr. 03, 2023. [Online]. Available: https://re.jrc.ec.europa.eu/pvg_tools/en/#TMY
[46] M. Coello and L. Boyle, "Simple Model for Predicting Time Series Soiling of Photovoltaic Panels," *IEEE Journal of Photovoltaics*, vol. 9, no. 5, pp. 1382–1387, Sep. 2019, doi: 10.1109/JPHOTOV.2019.2919628.
[47] W. F. Holmgren, C. W. Hansen, and M. A. Mikofski, "pvlib python: a python package for modeling solar energy systems," *Journal of Open Source Software*, vol. 3, no. 29, p. 884, Sep. 2018, doi: 10.21105/joss.00884.
[48] L. Micheli, F. Almonacid, J. G. Bessa, Á. Fernández-Solas, and E. F. Fernández, "The impact of extreme dust storms on the national photovoltaic energy supply," *Sustainable Energy Technologies and Assessments*, vol. 62, p. 103607, Feb. 2024, doi: 10.1016/j.seta.2024.103607.
[49] J. G. Bessa, L. Micheli, F. Almonacid, and E. F. Fernández, "Monitoring photovoltaic soiling: assessment, challenges, and perspectives of current and potential strategies," *iScience*, vol. 24, no. 3, p. 102165, Mar. 2021, doi: 10.1016/j.isci.2021.102165.
[50] "Climate reanalysis | Copernicus." Accessed: Jan. 30, 2022. [Online]. Available: https://climate.copernicus.eu/climate-reanalysis
[51] "CAMS global reanalysis (EAC4)." Accessed: Jan. 21, 2024. [Online]. Available: https://ads.atmosphere.copernicus.eu/cdsapp#!/dataset/cams-global-reanalysis-eac4?tab=overview
[52] B. Aboagye, S. Gyamfi, E. A. Ofosu, and S. Djordjevic, "Characterisation of degradation of photovoltaic (PV) module technologies in different climatic zones in Ghana," *Sustainable Energy Technologies and Assessments*, vol. 52, p. 102034, Aug. 2022, doi: 10.1016/j.seta.2022.102034.
[53] A. Louwen, S. Lindig, G. Chowdhury, and D. Moser, "Climate- and Technology-Dependent Performance Loss Rates in a Large Commercial Photovoltaic Monitoring Dataset," *Solar RRL*, vol. 8, no. 5, p. 2300653, 2024, doi: 10.1002/solr.202300653.
[54] "Bifacial Trackers, the real deal | Soltec." Accessed: May 07, 2024. [Online]. Available: https://soltec.com/en/innovation/lab/bifacial-trackers/
[55] K. R. McIntosh *et al.*, "Irradiance on the upper and lower modules of a two-high bifacial tracking system," in *2020 47th IEEE Photovoltaic Specialists Conference (PVSC)*, Jun. 2020, pp. 1916–1923. doi: 10.1109/PVSC45281.2020.9300838.
[56] M. Alam, M. S. Gul, and T. Muneer, "Performance analysis and comparison between bifacial and monofacial solar photovoltaic at various ground albedo conditions," *Renewable Energy Focus*, vol. 44, pp. 295–316, Mar. 2023, doi: 10.1016/j.ref.2023.01.005.
[57] W. Gu, S. Li, X. Liu, Z. Chen, X. Zhang, and T. Ma, "Experimental investigation of the bifacial photovoltaic module under real conditions," *Renewable Energy*, vol. 173, pp. 1111–1122, Aug. 2021, doi: 10.1016/j.renene.2020.12.024.
[58] F. Kersten *et al.*, "Degradation of multicrystalline silicon solar cells and modules after illumination at elevated temperature," *Solar Energy Materials and Solar Cells*, vol. 142, pp. 83–86, Nov. 2015, doi: 10.1016/j.solmat.2015.06.015.
[59] M. Woodhouse, I. Repins, and D. Miller, "LID and LeTID Impacts to PV Module Performance and System Economics: Draft Analysis," National Renewable Energy Lab. (NREL), Golden, CO (United States), NREL/PR-6A20-78629, Dec. 2020. Accessed: Jun. 20, 2024. [Online]. Available: https://www.osti.gov/biblio/1756712
[60] B. Adothu, S. Chattopadhyay, P. Bhatt, P. Hui, F. R. Costa, and S. Mallick, "Early-stage identification of encapsulants photobleaching and discoloration in crystalline silicon photovoltaic module laminates," *Progress in Photovoltaics: Research and Applications*, vol. 28, no. 8, pp. 767–778, 2020, doi: 10.1002/pip.3269.